

**Proximity-Induced Superconductivity with Subgap Anomaly in Type II Weyl
Semi-Metal WTe₂**

Qiao Li[†], Chaocheng He[†], Yaojia Wang[†], Erfu Liu[†], Miao Wang[†], Yu Wang[†], Junwen Zeng[†], Zecheng Ma[†], Tianjun Cao[†], Changjiang Yi[‡], Naizhou Wang^{§,†}, Kenji. Watanabe[⊥], Takashi. Taniguchi[⊥], Lubing Shao[†], Youguo Shi[‡], Xianhui Chen^{§,†}, Shi-Jun Liang^{*,†}, Qiang-Hua Wang^{*,†}, Feng Miao^{*,†}

[†] National Laboratory of Solid State Microstructures, School of Physics, Collaborative Innovation Center of Advanced Microstructures, Nanjing University, Nanjing 210093, China.

[‡] Institute of Physics, Chinese Academy of Sciences, Beijing 100190, China.

[§] Hefei National Laboratory for Physical Science at Microscale and Department of Physics, University of Science and Technology of China, Hefei, Anhui 230026, China.

[⊥] Key Laboratory of Strongly Coupled Quantum Matter Physics, University of Science and Technology of China, Hefei, Anhui 230026, China.

[⊥] National Institute for Materials Science, 1-1 Namiki Tsukuba, Ibaraki 305-0044, Japan.

Corresponding Authors

*Tel: +86-025-83621497. Fax: +86-025-83621497. E-mail: miao@nju.edu.cn (F. M.); qhwang@nju.edu.cn (Q. H. W.); sjliang@nju.edu.cn (S. J. L.).

ABSTRACT: Due to the non-trivial topological band structure in type-II Weyl semimetal Tungsten ditelluride (WTe_2), unconventional properties may emerge in its superconducting phase. While realizing intrinsic superconductivity has been challenging in the type-II Weyl semimetal WTe_2 , proximity effect may open an avenue for the realization of superconductivity. Here, we report the observation of proximity-induced superconductivity with a long coherence length along c axis in WTe_2 thin flakes based on a $\text{WTe}_2/\text{NbSe}_2$ van der Waals heterostructure. Interestingly, we also observe anomalous oscillations of the differential resistance during the transition from superconducting to normal state. Theoretical calculations show excellent agreement with experimental results, revealing that such a sub-gap anomaly is the intrinsic property of WTe_2 in superconducting state induced by the proximity effect. Our findings enrich the understanding of superconducting phase of type-II Weyl semimetals, and pave the way for their future applications in topological quantum computing.

KEYWORDS: WTe_2 , Superconductivity, Proximity effect, Sub-gap anomaly

Weyl semimetal, hosting low-energy quasiparticle excitations - Weyl fermions¹, is a new phase of matter with non-trivial topological band structure²⁻⁴. With linear band crossings around pairs of Weyl points (also called Weyl cones) and an open Fermi arc in surface state^{2, 5-7}, Weyl semimetals exhibit many unique properties, such as chiral anomaly⁸⁻¹² and anomalous Hall effect¹³. In addition, the multiple pairs of Weyl cones in the topological band structure may facilitate the formation of intra-cone pairing state with finite momentum and give rise to topological superconductivity¹⁴⁻²⁶ in Weyl semimetals when entering superconducting phase, which holds promise for fault-tolerant topological quantum computation. Thus, the potential realization of topological superconductivity in Weyl semimetals has sparked intense research interest.

Comparing to Type-I Weyl semimetals with a closed point-like Fermi surface, type-II Weyl semimetals possess unique features such as tilted Weyl cone-like energy spectrum and paired Weyl nodes formed at the boundary of electron and hole pockets²⁷⁻³¹, which lead to planar orientation-dependent chiral anomaly³². More interestingly, a type-II Weyl semimetal is expected to exhibit distinctive superconducting properties from type-I Weyl semimetals due to the tilted Weyl cone energy spectrum³³. As a typical type-II Weyl semimetal²⁷, Tungsten ditelluride (WTe₂) possesses distorted structure of T_d phase (space group Pnm2₁) which breaks the inversion symmetry and accommodates the existence of type-II Weyl points in film and topological edge state in monolayer³⁴⁻³⁹. With the unique topological bands, WTe₂ is expected to offer a platform to study topological superconductivity. However, the intrinsic superconductivity in exfoliated WTe₂ thin film has not yet been observed⁴⁰.

In this work, we report proximity effect induced superconductivity in thin WTe₂ flakes. The observed superconductivity is found to give rise to a long superconducting coherence length (above 30 nm) in WTe₂ along its *c* axis. In addition, we observe anomalous oscillations in the differential resistance spectra as the bias current drives the system from superconducting to normal state. Moreover, our theoretical calculations show that the anomaly could be associated with the sub-gap features in the density of states (DOS) spectra in superconducting WTe₂. Our work enriches the

understanding of superconducting phase in type-II Weyl semimetals and paves the way towards further exploration of topological superconducting states.

To realize proximity-induced superconductivity, a high-quality interface between thin WTe_2 flake and superconductor is desirable. To that end, we chose layered niobium diselenide (NbSe_2) as the superconductor (with $T_c \sim 7.2$ K and $\Delta \sim 1.2$ meV⁴¹) and fabricated $\text{WTe}_2/\text{NbSe}_2$ van der Waals heterostructure via dry-transfer method (see Methods for details)⁴². To avoid device degradation, both NbSe_2 and WTe_2 samples were exfoliated and transferred onto pre-prepared electrodes in glovebox. The whole heterostructure was further covered by a hexagonal Boron Nitride (h-BN) flake to avoid undesirable oxidation (as shown in Figure 1b). In the fabrication process, we selected the thin WTe_2 flakes with thickness of around 10 nm, to make sure that the flake was thick enough to exhibit band structures of type-II Weyl semimetal and thin enough to facilitate superconducting proximity effect. Besides, thin NbSe_2 flake (around 20 nm) with smaller area than WTe_2 sample was chosen to avoid NbSe_2 contacting with electrodes.

We first examined the low temperature transport properties of thin WTe_2 flakes by using a four-probe lock-in setup (with an AC current of 1 μA) (see Figure 1b). As shown in Figure 1c, we observe that the resistance of a typical device sharply drops to zero at a T_c (critical temperature) of 6.4 K at zero magnetic field, thus the superconducting phase in WTe_2 is achieved, which has been verified in a different device setup (see the part I in Supporting Information). As the applied perpendicular magnetic field increases, the critical temperature T_c reduces until the superconductivity is completely suppressed at around 5 T. The magnetoresistance curves at four different temperatures ($T=1.57, 3, 5$ and 7 K) are shown in Figure 1d. As temperature arises, the critical magnetic field becomes smaller. When the temperature increases to 7 K, the superconductivity disappears. A feature of weak anti-localization effect in the nonlinear magnetoresistance curve was then observed, similar to what has been reported in the normal resistance state of WTe_2 ⁴³. Note that the proximity effect induced superconductivity in this work is related to the intrinsic band structure of WTe_2 as a

type-II Weyl semimetal, different from high pressure-induced superconductivity in the 1T' phase WTe₂⁴⁴⁻⁴⁷ and superconductivity in the epitaxial WTe₂ thin film on a sapphire substrate⁴⁸.

The achievement of superconductivity in the 10 nm-thick sample implies a long superconducting coherence length along *c* axis in WTe₂. Based on the measured mobility along *a* axis $\mu \sim 2100 \text{ cm}^2/\text{V}^{-1}\text{s}^{-1}$ (see Fig.S6 in Supporting Information), the mobility along *c* axis is estimated to be around $210 \text{ cm}^2/\text{V}^{-1}\text{s}^{-1}$ since it is one order magnitude smaller than that along *a* axis⁴⁹. Combining the Fermi momentum $k_F \sim 1.2 \text{ nm}^{-1}$ along *c* axis⁴⁹, the mean free path (l_N) along *c* axis in WTe₂ is calculated to be around 18 nm (according to $\mu = el/\hbar k_F$), which is larger than the superconducting coherence length (ξ_S) (2.3 nm) along *c* axis of NbSe₂⁵⁰. In the “clean limit” (i.e. $\xi_S \ll l_N$)⁵¹, the superconducting coherence length in WTe₂ ξ_N can be calculated by $\xi_N(T) = \hbar v_N/2\pi k_B T$, where \hbar and k_B represent Planck constant and Boltzmann constant respectively, v_N is the Fermi velocity ($1.7 \times 10^5 \sim 3.1 \times 10^5 \text{ m/s}$ ^{52, 53}) and T is the temperature (6.4 K). ξ_N is estimated to be above 30 nm, which results from the intrinsic band structure of superconducting WTe₂ as a type-II Weyl semimetal, and will be discussed later.

To further investigate the proximity-induced superconducting properties in WTe₂, we performed differential resistance measurements (dV/dI vs. V) at various temperatures, with typical results shown in Figure 2a. Interestingly, we observe an anomalous feature in the differential resistance spectra when the temperature is below T_c . In the differential resistance spectrum, besides two remarkable symmetric peaks appearing as expected at around 280 μV , several small peaks emerge at lower voltage biases. Similar differential resistance spectrum has been observed in other samples (see Fig.S7 in Supporting Information). Different from that dV/dI vs. V_{ds} curve represents superconducting gap in conventional N/S junction, here, by applying an AC excitation current of 1 nA added on top of a variable DC bias current, dV/dI spectrum in this paper implies how WTe₂ resistance changes as the bias current drives WTe₂ from superconducting state to normal state. As temperature rises, these small peaks shrink in

both amplitude and bias gradually, and eventually vanish together with two main peaks after reaching T_c (6.4 K). The I - V characteristics at different temperatures can be obtained after integrating dV/dI - I curves, with results shown in Figure 2b. With increasing temperature, the superconductivity is completely suppressed at $T_c \sim 6.4$ K, which agrees well with the differential resistance spectra. At 1.6 K, zero-resistance state occurs at a critical current $I_c \sim 125 \mu\text{A}$ (I_c is defined as the current at which the voltage reduces to zero), and superconductivity in WTe_2 is suppressed at $I \sim 220 \mu\text{A}$. Moreover, the measured I_c (around $125 \mu\text{A}$ at $R_N \sim 2.5 \Omega$, with R_N defined as the sample resistance above T_c) of the device is one order of magnitude smaller than the I_c (1.8 mA at $R_N \sim 1 \Omega$) of NbSe_2 and this has been observed in other measured devices (see Table.S1 and Fig.S5 in the Supporting Information). Furthermore, the nonlinear variation of I - V curve between superconducting and normal state is slowly-varying, which is quite different from the abrupt change in NbSe_2 .

To shed light on the observed anomaly during the transition from superconducting to normal state, we further investigated the magnetic field dependence of the differential resistance spectra and I - V characteristics at $T=1.6$ K (See Figure 2c and 2d). Exceptionally, we find that the two main peaks become broad as B increases within small magnetic field range (lower than 0.1 T), in contrast to the temperature-induced behavior. Furthermore, we observe that all sub-features in spectra vanish at 0.3 T and that only two broad symmetric peaks are retained. Similarly, I - V characteristics (in Figure 2d) at various magnetic fields can be obtained by integrating the dV/dI - I curves. At lower magnetic fields, the I - V curves also show two current points indicating critical current and transition to normal state. At higher magnetic fields, the linear parts indicating the normal state in I - V curves are obviously separated by various magnetic fields, consistent with the magnetic field dependence of normal resistance of WTe_2 .

We calculated the DOS of type-II Weyl semimetal and s-wave superconductor in the $\text{WTe}_2/\text{NbSe}_2$ heterostructure to understand the anomalous experimental features of dV/dI spectra with results shown in the Figure 3a. WTe_2 and NbSe_2 , respectively, are simulated by an effective two-orbital model with spin-orbital coupling and a simple

one-orbital model with s-wave pairing in the inset of Figure 3a. (The calculation methods can be seen in the Supporting Information). We assume that there is no pairing potential in T_d-phase WTe₂, and that all of its superconducting behaviors are induced by coupling to the NbSe₂ superconductor. The DOS in superconducting NbSe₂ (blue line) is U-shaped, which is a feature of s-wave superconductor. However, the DOS (red line) in superconducting WTe₂ develops two coherence peaks at $E = \pm 0.25\Delta$, roughly one fourth of the gap in NbSe₂, which is identified as the induced superconducting gap of WTe₂. To have a closer view, we enlarge and replot the DOS of superconducting WTe₂ in Figure 3b. Inside the induced gap, we observe spiky sub-gap features consistent with the observed sub-features in the dV/dI vs V spectra in the Figure 2b and 2d. Besides, our theoretical calculations show that the gap features persist beyond ten layers in the WTe₂ while similar features already vanish in a type-I Weyl semimetal beyond the second layer (See Fig.S11 in the Supporting Information). We speculate that this may be related to the fact that the electron and hole pockets in WTe₂ provide larger DOS at the Fermi energy for electrons to pair up in proximity to the bulk superconductor, leading to a longer coherence length along c axis as aforementioned.

Based on the calculated results, we can understand the sub-gap anomaly observed in the differential resistance spectra in the following way. The total current in the sample is composed of the supercurrent and normal current when the bias current goes beyond the critical current. The dissipative normal current is carried by quasi-particles, which are excited by breaking the Cooper pairs self-consistently via the voltage drop induced by the normal current (as well as the Doppler shift effect in the presence of the current). The induced gap on the electron and hole Fermi pockets of WTe₂ is non-uniform, as evidenced by the peaks in DOS in Figure 3b (red line). The Cooper pair-breaking is a multiple-step process and starts from the smaller gap, instead of in an abrupt way as in conventional superconductors. The de-pairing of Cooper pairs at voltages corresponding to the DOS peaks excites a relatively larger number of quasiparticles, and the dissipative component of the total driving current will be enhanced, leading to an enhancement of the differential resistance. We emphasize that the voltage is

measured under a bias current in our case, which is different from the usual case in which current is measured in response to a bias voltage.

To further prove that the unusual differential resistance spectra of superconducting WTe_2 thin flake root in the unique DOS of WTe_2 , we carried out both theoretical and experimental studies on graphene/ NbSe_2 device with 10 nm thick graphene flake (the device structure is shown in the inset of Figure 4b). We first calculated the DOS of the graphene and NbSe_2 , with results shown in Figure 4a. The DOS of graphene resembles that of superconducting NbSe_2 but differs from that of superconducting WTe_2 . We then measured the resistance of the graphene thin flake in a typical graphene/ NbSe_2 device at various temperatures. As shown in Figure 4b, with decreasing temperature, superconductivity can be also achieved in graphene at a transition temperature T_c of around 6.3 K, close to that of NbSe_2 . In contrast to the magnetoresistance results in WTe_2 , the normal resistance of graphene thin flake remains almost constant over the applied magnetic field range, which is consistent with the suppression of weak localization in graphene thin flake⁵⁴. We further measured the differential resistance spectra at various temperatures and magnetic fields (see Figure 4c and Figure 4d). As expected, only two neat peaks are present in the scanning current range, without any sub-peaks emerging. When increasing temperature or magnetic field, the two peaks behave similarly to that of WTe_2 .

Compared with the properties of superconducting graphene, the DOS of WTe_2 in the superconducting state is indeed unique and shows consistency with the experimental results. The trivial dV/dI spectra of graphene without any sub-peaks would result in one-step increase in resistance when driving superconducting to normal state. Such usual behavior indicates that Cooper pairs are broken into quasiparticles in an abrupt manner, different from multiple-step process occurring in the superconducting WTe_2 thin flake. Combining all the evidence above, we believe that the nontrivial signature in the dV/dI spectra of WTe_2 is unique and roots in its intrinsic band structure. Note that the sub-gap features in WTe_2 may occur in another type-II Weyl semimetal MoTe_2 ⁵⁵,

thus this should stimulate further exploration of the properties of type-II Weyl semimetals in superconducting phase.

In summary, we achieve superconductivity for the first time in type-II Weyl semimetal WTe_2 by proximity effect based on a $WTe_2/NbSe_2$ heterostructure. The superconducting transition occurs at 6.4 K in WTe_2 , close to T_c of $NbSe_2$. Most importantly, we discover anomalous oscillations of dV/dI spectra in superconducting WTe_2 . Furthermore, our theoretical calculations confirm that such peculiar feature in the dV/dI spectra in superconducting WTe_2 results from its nontrivial DOS spectrum. This work suggests that superconductivity in type-II Weyl semimetals exhibits distinctive feature from conventional superconductors and will stimulate further interest in exploration of topological superconductivity.

We grew the high-quality $NbSe_2$ single crystals with a standard chemical vapor transport method. High purity powders of elements Nb and Se are stoichiometric mixed and thoroughly grounded. Then the mixture was sealed under vacuum in a quartz tube with iodine (5mg cm^{-3}). The tube was placed into a two-zone horizontal furnace with the hot end of $780\text{ }^\circ\text{C}$ and the cold end of $700\text{ }^\circ\text{C}$ for two weeks. High-quality plate-like $NbSe_2$ single crystals are obtained.

Single crystals of WTe_2 were grown by a high temperature self-flux method. High-purity W powders (99.9%) and Te pieces (99.999%) were put in alumina crucibles with a molar ratio of 1:30 in a glove box filled with pure argon then sealed in quartz tubes under high vacuum. The tubes were heated to 1373 K and maintained for 10 hours. Then the furnace was slowly cooled down to 923 K with a rate of 2 K/h followed by separating the Te flux in a centrifuge at 923 K.

We mechanically exfoliated h-BN onto a highly doped Si wafer covered by a 300-nm-thick SiO_2 layer. The bottom electrodes (5 nm Ti/40nm Au) were patterned on h-BN flake using standard electron beam lithography method and deposited by standard electron beam evaporation. The WTe_2 , $NbSe_2$ and graphene thin flakes were

mechanically exfoliated from single crystals onto the PDMS (Polydimethylsiloxane) substrate in a glove box filled with an inert atmosphere, followed by dry transferring on the top of bottom electrodes layer by layer. Finally, a Boron Nitride thin flake was transferred on to WTe₂/NbSe₂ heterostructure to avoid the device degradation in the air. All the transfer processes mentioned above were finished in the glove box to achieve the best quality of the device. Bruker Multimode 8 atomic force microscopy was used to identify the thickness of WTe₂, NbSe₂ and graphene thin flakes.

The devices were measured in an Oxford cryostat with a base temperature of about 1.6 K. The resistance signals were collected using a low-frequency Lock-in amplifier. The differential resistance signals were collected by applying an AC excitation current of 1 nA added on top of a variable DC bias current.

ASSOCIATED CONTENT

Supporting information

The Supporting information is available free of charge on the ACS Publications website at <http://pubs.acs.org>.

Superconductivity in WTe₂/NbSe₂ heterostructure with a trench in NbSe₂ layer; Low-temperature electrical transport properties of NbSe₂ under different temperatures and magnetic fields; Mobility for WTe₂ encapsulated by BN flakes; Critical current and observation of sub-gap anomaly in other WTe₂ samples; Theoretical calculation methods for DOS of s-wave superconductor (NbSe₂) and Weyl semimetals (WSM); DOS spectra of NbSe₂ and type-I Weyl semimetal; *I-V* characteristics of graphene thin flake under various temperatures and magnetic fields.

AUTHOR INFORMATION

Corresponding Authors

*Tel: +86-025-83621497. Fax: +86-025-83621497. E-mail: miao@nju.edu.cn (F. M.); qhwang@nju.edu.cn (Q. H. W.); sjliang@nju.edu.cn (S. J. L.).

Notes

The authors declare no competing financial interests.

Acknowledgements

This work was supported in part by the National Key Basic Research Program of China (2015CB921600), the National Natural Science Foundation of China (61625402, 61574076, 11774399, 11474330, 11574134, 11534010), the Key Research Program of Frontier Sciences CAS (Grant No. QYZDY-SSW-SLH021), the National Key Research and Development Program of China (2016YFA0300401, 2017YFA0302901, 2016YFA0300604), Fundamental Research Funds for the Central Universities (020414380093, 020414380084), the Collaborative Innovation Center of Advanced Microstructures and Natural Science Foundation of Jiangsu Province (BK20180330). K.W. and T.T. acknowledge support from the Elemental Strategy Initiative conducted by the MEXT, Japan and the CREST (JPMJCR15F3), JST.

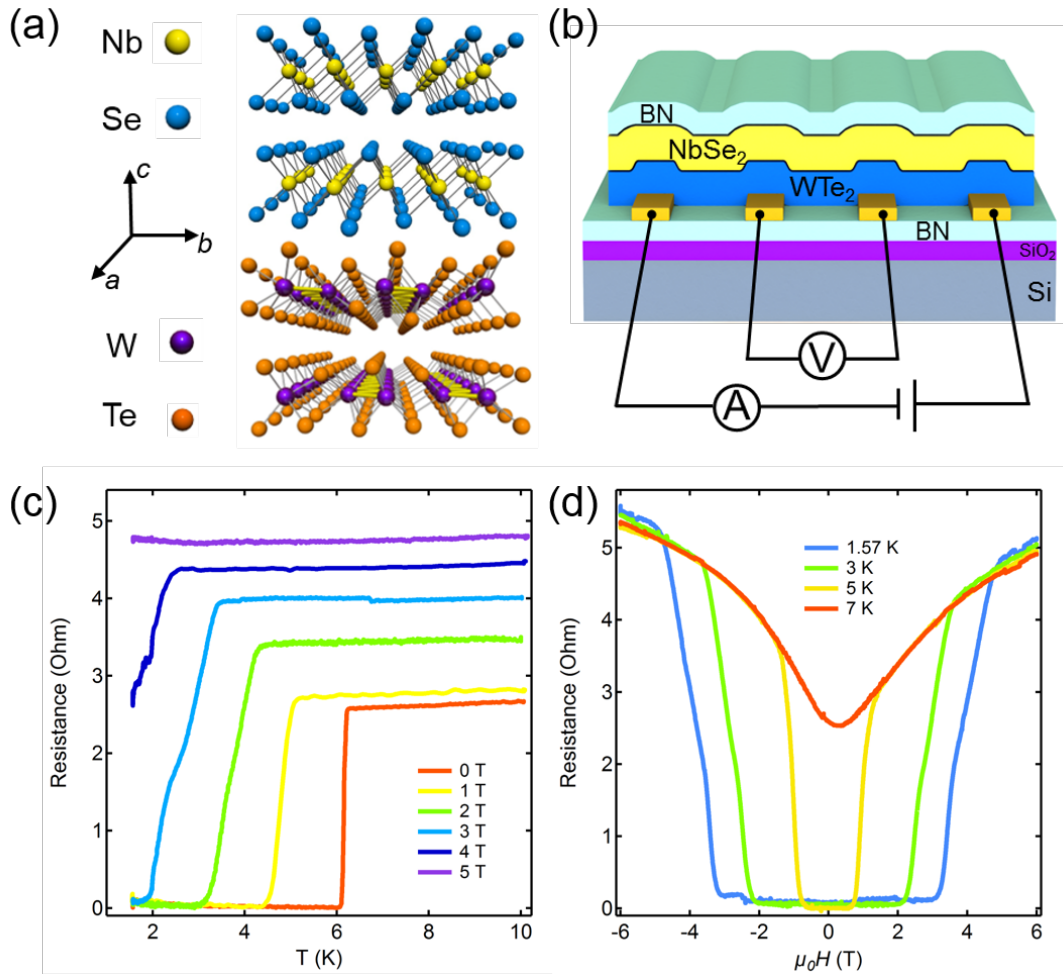


Figure 1. WTe₂/NbSe₂ device and basic superconducting characterizations of WTe₂. (a) Crystal structure of WTe₂ and NbSe₂. (b) Schematic structure and measurement setup of a four-probe WTe₂/NbSe₂ device. (c) R - T curves of WTe₂ channel at different applied perpendicular magnetic fields. (d) R - $\mu_0 H$ curves of WTe₂ channel measured at various temperatures. The magnetoresistance above T_c acts like weak anti-localization of WTe₂.

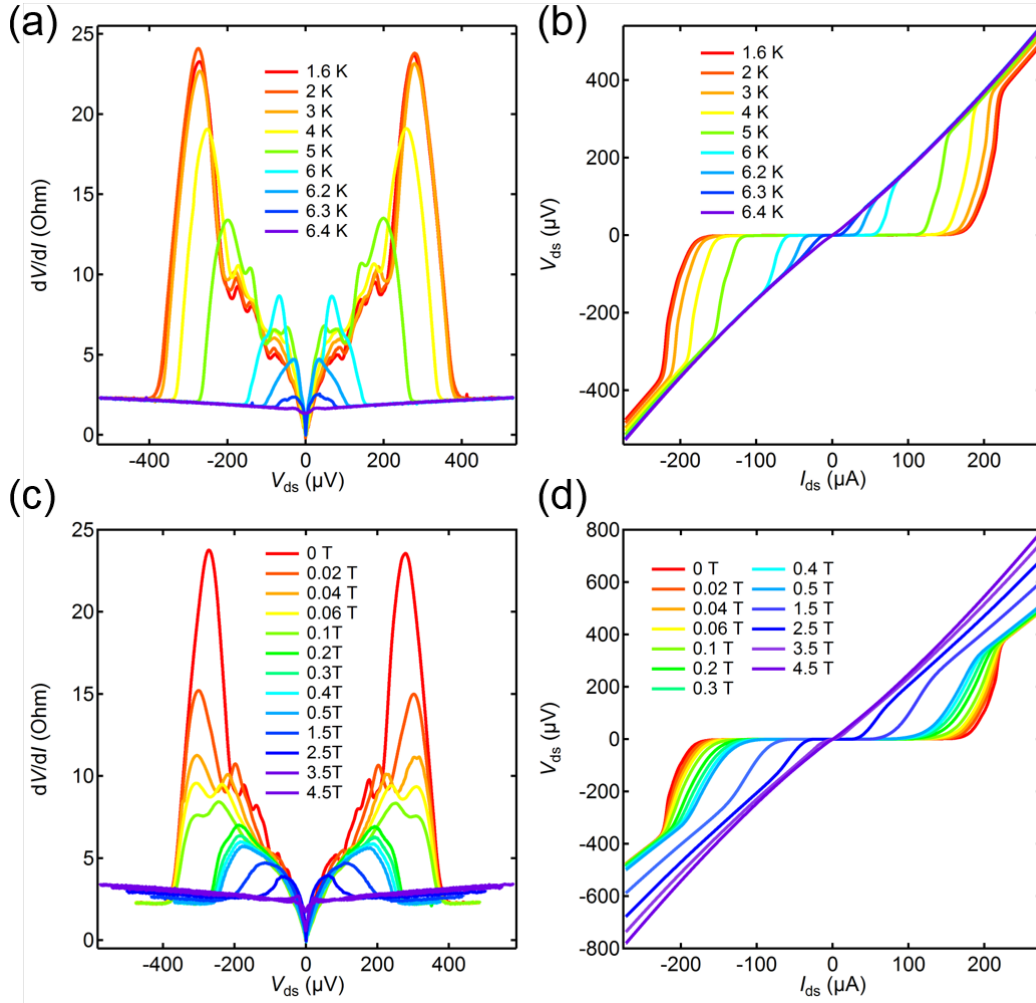


Figure 2. Differential resistance spectra and Current-Voltage (I-V) curves of WTe₂. (a) Differential resistance spectra of WTe₂ measured at various temperatures. Several smaller peaks emerge inside of two main peaks. (b) I - V curves of WTe₂ at different temperatures ranging from 1.6 K to 6.4 K without applying magnetic field. (c) Differential resistance spectra of WTe₂ measured at various applied magnetic fields at 1.6 K. (d) I - V curves of WTe₂ at different applied magnetic fields ranging from 0 T to 4.5 T.

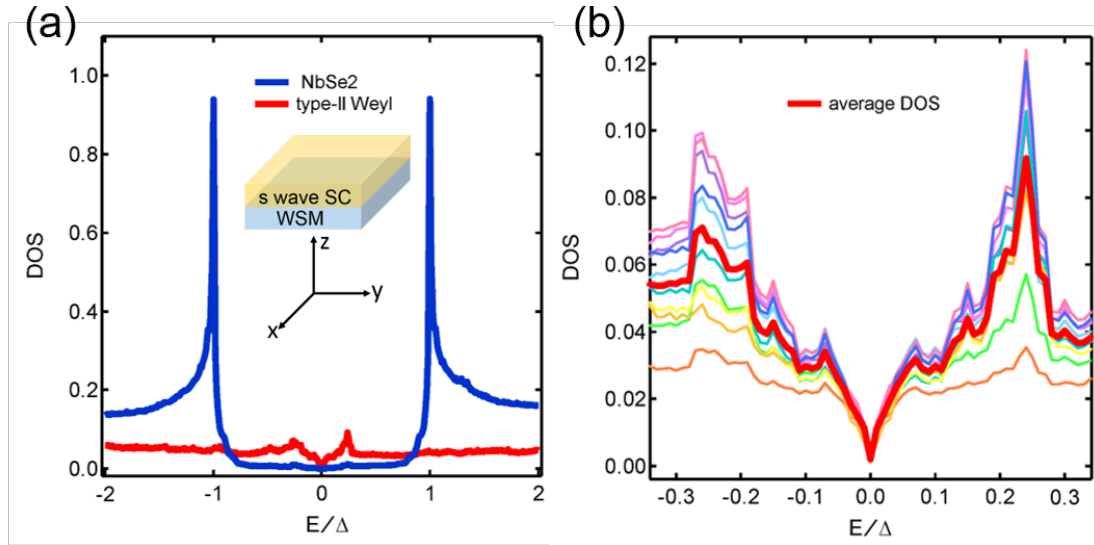


Figure 3. Theoretical calculations of density of states in superconducting $WTe_2/NbSe_2$ heterostructure. (a) Density of states (DOS) spectra (in arb. unit) versus energy E (normalized by the maximal gap Δ) of type-II Weyl semimetal (WTe_2) and s-wave superconductor ($NbSe_2$) in superconducting state. $E/\Delta=1$ is the superconducting gap we included in the calculations. Inset shows schematic drawing of theoretical calculation model. (b) Enlarged DOS spectra of WTe_2 in (a) (red line). Thin curves represent DOS of different layers in WTe_2 .

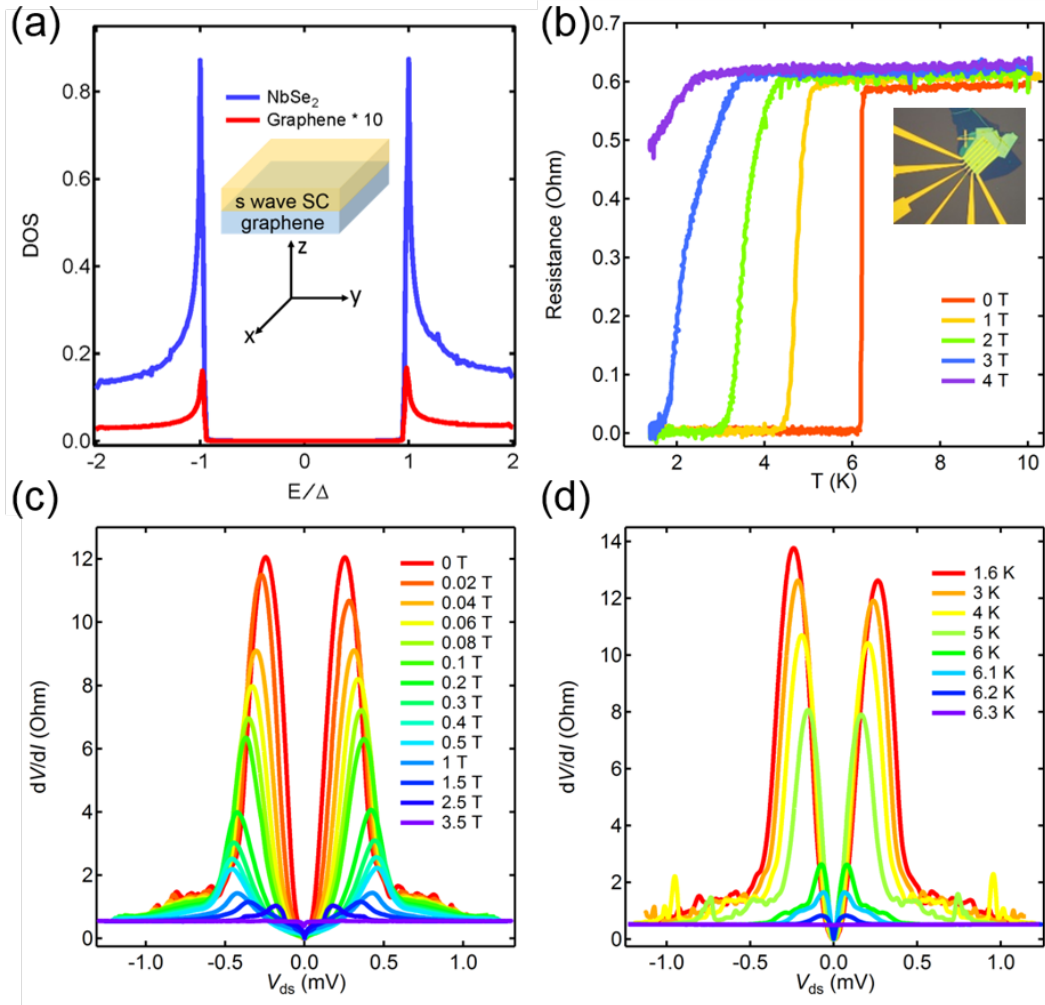


Figure 4. Theoretical calculations and experimental data of graphene thin flake. (a) DOS of graphene thin flake and NbSe_2 in superconducting state, showing a trivial (DOS) signature. Inset: schematic drawing of theoretical calculation model. (b) R - T characteristics of graphene thin flake (around 10 nm) at various magnetic fields ranging from 0 T to 4 T. Inset: optical image of graphene/ NbSe_2 heterostructure device. (c) Differential resistance spectra of graphene thin flake at different temperatures. The straight line at 6.4 K indicates that the superconductivity is completely suppressed. (d) Differential resistance spectra of graphene thin flake at different applied magnetic fields.

References:

- (1) Weyl, H. Elektron und gravitation. I. *Zeitschr. Phys.* **1929**, 56, 330-352.
- (2) Wan, X.; Turner, A. M.; Vishwanath, A.; Savrasov, S. Y. Topological semimetal and Fermi-arc surface states in the electronic structure of pyrochlore iridates. *Phys. Rev. B* **2011**, 83, 205101.
- (3) Burkov, A. A.; Balents, L. Weyl Semimetal in a Topological Insulator Multilayer. *Phys. Rev. Lett.* **2011**, 107, 127205.
- (4) Weng, H.; Fang, C.; Fang, Z.; Bernevig, B. A.; Dai, X. Weyl Semimetal Phase in Noncentrosymmetric Transition-Metal Monophosphides. *Phys. Rev. X* **2015**, 5, 011029.
- (5) Murakami, S. Phase transition between the quantum spin Hall and insulator phases in 3D: emergence of a topological gapless phase. *New J. Phys.* **2007**, 9, 356.
- (6) Xu, S.; Belopolski, I.; Alidoust, N.; Neupane, M.; Bian, G.; Zhang, C.; Sankar, R.; Chang, G.; Yuan, Z.; Lee, C.; Huang, S.; Zheng, H.; Ma, J.; Sanchez, D. S.; Wang, B.; Bansil, A.; Chou, F.; Shibaev, P. P.; Lin, H.; Jia, S.; Hasan, M. Z. Discovery of a Weyl fermion semimetal and topological Fermi arcs. *Science* **2015**, 349, 613-617.
- (7) Lv, B. Q.; Weng, H. M.; Fu, B. B.; Wang, X. P.; Miao, H.; Ma, J.; Richard, P.; Huang, X. C.; Zhao, L. X.; Chen, G. F.; Fang, Z.; Dai, X.; Qian, T.; Ding, H. Experimental Discovery of Weyl Semimetal TaAs. *Phys. Rev. X* **2015**, 5, 031013.
- (8) Nielsen, H. B.; Ninomiya, M. The Adler-Bell-Jackiw anomaly and Weyl fermions in a crystal. *Phys. Rev. B* **1983**, 130, 389-396.
- (9) Kim, H.; Kim, K.; Wang, J. F.; Sasaki, M.; Satoh, N.; Ohnishi, A.; Kitaura, M.; Yang, M.; Li, L. Dirac versus Weyl Fermions in Topological Insulators: Adler-Bell-Jackiw Anomaly in Transport Phenomena. *Phys. Rev. Lett.* **2013**, 111, 246603.
- (10) Son, D. T.; Spivak, B. Z. Chiral anomaly and classical negative magnetoresistance of Weyl metals. *Phys. Rev. B* **2013**, 88, 104412.
- (11) Huang, X.; Zhao, L.; Long, Y.; Wang, P.; Chen, D.; Yang, Z.; Liang, H.; Xue, M.; Weng, H.; Fang, Z.; Dai, X.; Chen, G. Observation of the Chiral-Anomaly-Induced Negative Magnetoresistance in 3D Weyl Semimetal TaAs. *Phys. Rev. X* **2015**, 5, 031023.
- (12) Zhang, C.; Xu, S.; Belopolski, I.; Yuan, Z.; Lin, Z.; Tong, B.; Bian, G.; Alidoust, N.; Lee, C.; Huang, S.; Chang, T.; Chang, G.; Hsu, C.; Jeng, H.; Neupane, M.; Sanchez, D. S.; Zheng, H.; Wang, J.; Lin, H.; Zhang, C.; Lu, H.; Shen, S.; Neupert, T.; Hasan, M. Z.; Jia, S. Signatures of the Adler-Bell-Jackiw chiral anomaly in a Weyl fermion semimetal. *Nat. Commun.* **2016**, 7, 10735.
- (13) Burkov, A. A. Anomalous Hall effect in Weyl metals. *Phys. Rev. Lett.* **2014**, 113, 187202.
- (14) Wei, H.; Chao, S.; Aji, V. Odd-parity superconductivity in Weyl semimetals. *Phys. Rev. B* **2014**, 89, 014506.
- (15) Khanna, U.; Kundu, A.; Pradhan, S.; Rao, S. Proximity-induced superconductivity in Weyl semimetals. *Phys. Rev. B* **2014**, 90, 195430.
- (16) Hosur, P.; Dai, X.; Fang, Z.; Qi, X. Time-reversal-invariant topological superconductivity in doped Weyl semimetals. *Phys. Rev. B* **2014**, 90, 045130.
- (17) Lu, B.; Yada, K.; Sato, M.; Tanaka, Y. Crossed surface flat bands of Weyl semimetal superconductors. *Phys. Rev. Lett.* **2015**, 114, 096804.
- (18) Bednik, G.; Zyuzin, A. A.; Burkov, A. A. Superconductivity in Weyl metals. *Phys. Rev. B* **2015**, 92, 035153.
- (19) Bednik, G.; Zyuzin, A. A.; Burkov, A. A. Anomalous Hall effect in Weyl superconductors. *New J.*

Phys. **2016**, 18, 085002.

(20) Kim, Y.; Park, M. J.; Gilbert, M. J. Probing unconventional superconductivity in inversion-symmetric doped Weyl semimetal. *Phys. Rev. B* **2016**, 93, 214511.

(21) Chen, A.; Franz, M. Superconducting proximity effect and Majorana flat bands at the surface of a Weyl semimetal. *Phys. Rev. B* **2016**, 93, 201105.

(22) Zhou, T.; Gao, Y.; Wang, Z. D. Superconductivity in doped inversion-symmetric Weyl semimetals. *Phys. Rev. B* **2016**, 93, 094517.

(23) Rao, S. Weyl semi-metals: a short review. *J. Indian Inst. Sci* **2016**, 96, 145-156.

(24) Meng, T.; Balents, L. Weyl superconductors. *Phys. Rev. B* **2012**, 86, 054504.

(25) Hou, Z.; Sun, Q. Double Andreev reflections in type-II Weyl semimetal-superconductor junctions. *Phys. Rev. B* **2017**, 96, 155305.

(26) Chen, A.; Pikulin, D. I.; Franz, M. Josephson current signatures of Majorana flat bands on the surface of time-reversal-invariant Weyl and Dirac semimetals. *Phys. Rev. B* **2017**, 95, 174505.

(27) Soluyanov, A. A.; Gresch, D.; Wang, Z.; Wu, Q.; Troyer, M.; Dai, X.; Bernevig, B. A. Type-II Weyl semimetals. *Nature* **2015**, 527, 495-498.

(28) Sun, Y.; Wu, S.; Ali, M. N.; Felser, C.; Yan, B. Prediction of Weyl semimetal in orthorhombic MoTe₂. *Phys. Rev. B* **2015**, 92, 161107.

(29) Wang, Z.; Gresch, D.; Soluyanov, A. A.; Xie, W.; Kushwaha, S.; Dai, X.; Troyer, M.; Cava, R. J.; Bernevig, B. A. MoTe₂: A Type-II Weyl Topological Metal. *Phys. Rev. Lett.* **2016**, 117, 056805.

(30) Deng, K.; Wan, G.; Deng, P.; Zhang, K.; Ding, S.; Wang, E.; Yan, M.; Huang, H.; Zhang, H.; Xu, Z.; Denlinger, J.; Fedorov, A.; Yang, H.; Duan, W.; Yao, H.; Wu, Y.; Fan, S.; Zhang, H.; Chen, X.; Zhou, S. Experimental observation of topological Fermi arcs in type-II Weyl semimetal MoTe₂. *Nat. Phys.* **2016**, 12, 1105-1110.

(31) Huang, L.; McCormick, T. M.; Ochi, M.; Zhao, Z.; Suzuki, M.; Arita, R.; Wu, Y.; Mou, D.; Cao, H.; Yan, J.; Trivedi, N.; Kaminski, A. Spectroscopic evidence for a type II Weyl semimetallic state in MoTe₂. *Nat. Mater.* **2016**, 15, 1155-1160.

(32) Wang, Y.; Liu, E.; Liu, H.; Pan, Y.; Zhang, L.; Zeng, J.; Fu, Y.; Wang, M.; Xu, K.; Huang, Z.; Wang, Z.; Lu, H.; Xing, D.; Wang, B.; Wan, X.; Miao, F. Gate-tunable negative longitudinal magnetoresistance in the predicted type-II Weyl semimetal WTe₂. *Nat. Commun.* **2016**, 7, 13142.

(33) Alidoust, M.; Halterman, K.; Zyuzin, A. A. Superconductivity in type-II Weyl semimetals. *Phys. Rev. B* **2017**, 95, 155124.

(34) Wu, S.; Fatemi, V.; Gibson, Q. D.; Watanabe, K.; Taniguchi, T.; Cava, R. J.; Jarillo-Herrero, P. Observation of the quantum spin Hall effect up to 100 kelvin in a monolayer crystal. *Science* **2018**, 359, 76-79.

(35) Fei, Z.; Palomaki, T.; Wu, S.; Zhao, W.; Cai, X.; Sun, B.; Nguyen, P.; Finney, J.; Xu, X.; Cobden, D. H. Edge conduction in monolayer WTe₂. *Nat. Phys.* **2017**, 13, 677-682.

(36) Tang, S.; Zhang, C.; Wong, D.; Pedramrazi, Z.; Tsai, H.; Jia, C.; Moritz, B.; Claassen, M.; Ryu, H.; Kahn, S.; Jiang, J.; Yan, H.; Hashimoto, M.; Lu, D.; Moore, R. G.; Hwang, C.; Hwang, C.; Hussain, Z.; Chen, Y.; Ugeda, M. M.; Liu, Z.; Xie, X.; Devereaux, T. P.; Crommie, M. F.; Mo, S.; Shen, Z. Quantum spin Hall state in monolayer 1T'-WTe₂. *Nat. Phys.* **2017**, 13, 683-687.

(37) Xu, S.; Ma, Q.; Shen, H.; Fatemi, V.; Wu, S.; Chang, T.; Chang, G.; Valdivia, A. M. M.; Chan, C.; Gibson, Q. D.; Zhou, J.; Liu, Z.; Watanabe, K.; Taniguchi, T.; Lin, H.; Cava, R. J.; Fu, L.; Gedik, N.; Jarillo-Herrero, P. Electrically switchable Berry curvature dipole in the monolayer topological insulator WTe₂. *Nat. Phys.* **2018**, 14, 900-906.

- (38) Fatemi, V.; Wu, S.; Cao, Y.; Bretheau, L.; Gibson, Q. D.; Watanabe, K.; Taniguchi, T.; Cava, R. J.; Jarillo-Herrero, P. Electrically tunable low-density superconductivity in a monolayer topological insulator. *Science* **2018**, DOI: 10.1126/science.aar4642.
- (39) Sajadi, E.; Palomaki, T.; Fei, Z.; Zhao, W.; Bement, P.; Olsen, C.; Luescher, S.; Xu, X.; Folk, J. A.; Cobden, D. H. Gate-induced superconductivity in a monolayer topological insulator. *Science* **2018**, DOI: 10.1126/science.aar4426.
- (40) Cai, P. L.; Hu, J.; He, L. P.; Pan, J.; Hong, X. C.; Zhang, Z.; Zhang, J.; Wei, J.; Mao, Z. Q.; Li, S. Y. Drastic pressure effect on the extremely large magnetoresistance in WTe₂: quantum oscillation study. *Phys. Rev. Lett.* **2015**, 115, 057202.
- (41) Frindt, R. F. Superconductivity in Ultrathin NbSe₂ Layers. *Phys. Rev. Lett.* **1972**, 28, 299-301.
- (42) Novoselov, K. S.; Mishchenko, A.; Carvalho, A.; Castro Neto, A. H. 2D materials and van der Waals heterostructures. *Science* **2016**, 353, aac9439.
- (43) Wang, L.; Gutiérrez-Lezama, I.; Barreateau, C.; Ubrig, N.; Giannini, E.; Morpurgo, A. F. Tuning magnetotransport in a compensated semimetal at the atomic scale. *Nat. Commun.* **2015**, 6, 8892.
- (44) Pan, X.; Chen, X.; Liu, H.; Feng, Y.; Wei, Z.; Zhou, Y.; Chi, Z.; Pi, L.; Yen, F.; Song, F.; Wan, X.; Yang, Z.; Wang, B.; Wang, G.; Zhang, Y. Pressure-driven dome-shaped superconductivity and electronic structural evolution in tungsten ditelluride. *Nat. Commun.* **2015**, 6, 7805.
- (45) Kang, D.; Zhou, Y.; Yi, W.; Yang, C.; Guo, J.; Shi, Y.; Zhang, S.; Wang, Z.; Zhang, C.; Jiang, S.; Li, A.; Yang, K.; Wu, Q.; Zhang, G.; Sun, L.; Zhao, Z. Superconductivity emerging from a suppressed large magnetoresistant state in tungsten ditelluride. *Nat. Commun.* **2015**, 6, 7804.
- (46) Lu, P.; Kim, J.; Yang, J.; Gao, H.; Wu, J.; Shao, D.; Li, B.; Zhou, D.; Sun, J.; Akinwande, D.; Xing, D.; Lin, J. Origin of superconductivity in the Weyl semimetal WTe₂ under pressure. *Phys. Rev. B* **2016**, 94, 224512.
- (47) Zhou, Y.; Chen, X.; Li, N.; Zhang, R.; Wang, X.; An, C.; Zhou, Y.; Pan, X.; Song, F.; Wang, B.; Yang, W.; Yang, Z.; Zhang, Y. Pressure-induced T_d to 1T' structural phase transition in WTe₂. *AIP Adv.* **2016**, 6, 075008.
- (48) Asaba, T.; Wang, Y.; Li, G.; Xiang, Z.; Tinsman, C.; Chen, L.; Zhou, S.; Zhao, S.; Laleyan, D.; Li, Y.; Mi, Z.; Li, L. Magnetic Field Enhanced Superconductivity in Epitaxial Thin Film WTe₂. *Sci. Rep.* **2018**, 8, 6520.
- (49) Zhu, Z.; Lin, X.; Liu, J.; Fauque, B.; Tao, Q.; Yang, C.; Shi, Y.; Behnia, K. Quantum oscillations, thermoelectric coefficients, and the Fermi surface of semimetallic WTe₂. *Phys. Rev. Lett.* **2015**, 114, 176601.
- (50) de Trey, P.; Gygax, S.; Jan, J. P. Anisotropy of the Ginzburg-Landau parameter κ in NbSe₂. *J. Low Temp. Phys.* **1973**, 11, 421-434.
- (51) Bozovic, I.; Logvenov, G.; Verhoeven, M. A. J.; Caputo, P.; Goldobin, E.; Beasley, M. R. Giant proximity effect in cuprate superconductors. *Phys. Rev. Lett.* **2004**, 93, 157002.
- (52) Pan, X.; Pan, Y.; Jiang, J.; Zuo, H.; Liu, H.; Chen, X.; Wei, Z.; Zhang, S.; Wang, Z.; Wan, X.; Yang, Z.; Feng, D.; Xia, Z.; Li, L.; Song, F.; Wang, B.; Zhang, Y.; Wang, G. Carrier balance and linear magnetoresistance in type-II Weyl semimetal WTe₂. *Front. Phys.* **2017**, 12, 127203.
- (53) Li, P.; Wen, Y.; He, X.; Zhang, Q.; Xia, C.; Yu, Z.; Yang, S. A.; Zhu, Z.; Alshareef, H. N.; Zhang, X. Evidence for topological type-II Weyl semimetal WTe₂. *Nat. Commun.* **2017**, 8, 2150.
- (54) Morozov, S. V.; Novoselov, K. S.; Katsnelson, M. I.; Schedin, F.; Ponomarenko, L. A.; Jiang, D.; Geim, A. K. Strong suppression of weak localization in graphene. *Phys. Rev. Lett.* **2006**, 97, 016801.
- (55) Guguchia, Z.; von Rohr, F.; Shermadini, Z.; Lee, A. T.; Banerjee, S.; Wieteska, A. R.; Marianetti,

C. A.; Frandsen, B. A.; Luetkens, H.; Gong, Z.; Cheung, S. C.; Baines, C.; Shengelaya, A.; Taniashvili, G.; Pasupathy, A. N.; Morenzoni, E.; Billinge, S. J. L.; Amato, A.; Cava, R. J.; Khasanov, R.; Uemura, Y. J. Signatures of the topological s^+ superconducting order parameter in the type-II Weyl semimetal $T_d\text{-MoTe}_2$. *Nat. Commun.* **2017**, 8, 1082.

For TOC graphic only

